A Closed-Loop Fuzzy Logic Based Current Controller for PMSM Torque Ripple Minimization Using the Magnitude of Speed Harmonic as the Feedback Control Signal

Guodong Feng, *Member*, *IEEE*, Chunyan Lai, *Student Member*, *IEEE*, and Narayan C. Kar, *Senior Member*, *IEEE*

Abstract **– This paper investigates torque ripple minimization for permanent magnet synchronous machine (PMSM), and proposes a closed-loop fuzzy logic based current controller by using the magnitude of the speed harmonic as the feedback control signal. The speed harmonic can be obtained from machine speed measurement, so the proposed approach does not require accurate machine parameters and is not influenced by the nonlinearity of the machine and drive. The torque harmonic can produce the speed harmonic of the same order, so their relation is investigated, which shows that the magnitude of the speed harmonic is proportional to the magnitude of the torque harmonic of the same order, so it can be used as a measure of torque harmonic for torque ripple minimization. Then, the torque harmonic model is developed to facilitate the design and analysis of the current controller. Afterwards, a novel fuzzy logic based current controller is proposed to minimize the dominant torque harmonics. The proposed current controller is evaluated on a laboratory PMSM drive system under different load conditions and operation speeds.**

***Index Terms*— Feedback fuzzy logic controller, PMSM, speed harmonic, torque ripple modeling and minimization**

I. INTRODUCTION

TORQUE ripple minimization has received considerable research interests for permanent magnet synchronous machine (PMSM) drives. This is because torque ripple can generate mechanical vibration and acoustic noise, degrade the machine drive performance and prevent the machine from the applications that require accurate controls such as robotic systems [1-5]. In the literature, the torque ripple minimization approaches can be mainly divided into two categories, namely, the machine design approach and machine control approach. The machine design approach focuses on machine stator and rotor design to optimize the cogging torque and spatial harmonics of magnet flux [6, 7]. While the machine control approach investigates the optimization of the excitation current waveforms to cancel the torque ripple and generate a smooth output torque [8-12]. This paper studies the machine control approach and proposes a novel closed-loop fuzzy logic based current controller for torque ripple minimization.

The key to machine control approach is to determine an optimal current waveform that can generate extra torque ripples to cancel the cogging torque and the torque ripples caused by flux harmonics [13-15]. Machine control approach can be furthered divided into the feedforward compensation approach and the feedback control approach.

The feedforward compensation approach requires accurate torque ripple model to determine the optimal current waveform. For instance, in [8], a neural network based approach is proposed to calculate the optimal stator current, which requires accurate machine parameters such as magnet flux to model the torque ripples. However, modeling and prediction of torque ripple is often challenging due to magnetic saturation, temperature issue and nonlinearity of machine drives [16-23]. Offline test and FEA based methods can also be used to model the torque ripple. However, offline test is often time-consuming and difficult to cover all operation conditions, while FEA simulation requires accurate geometric information which is not always available.

The feedback control approach is based on the torque estimation for feedback current control to suppress the torque ripples. This approach relies on accurate torque estimator /observer. For instance, in [24], a torque predictive control is proposed to minimize the torque ripple. However, the torque estimator/observer requires accurate machine model and thus this approach is sensitive to the variation of machine parameters, which is inevitable due to the nonlinearity of the machine and drives. The reason behind is that there are lacking an effective torque ripple measure that is independent from the machine, because the torque transducer is usually expensive to be used in machine drive.

Recently, the piezoelectric vibration sensor has gained much attention for torque ripple minimization [25-27]. This sensor can be installed on the motor base to measure the torque ripple induced vibration. This vibration can be used as a measure of the torque ripple for feedback current control to minimize the torque ripple. Besides, some other researches focus on using the speed errors for torque ripple minimization, because the speed ripples are induced by the torque ripples [28, 29]. For instance, in [29], the speed errors are used as the feedback control signal, and an iterative learning control scheme is proposed for current control. However, the speed error contains certain harmonics that are not induced by the torque ripples, and thus this method is sensitive to the non-integer and pseudo harmonics in the speed measurements.

This paper explores the use of the speed harmonic magnitude as the feedback control signal for torque harmonic minimization. The speed harmonic can be obtained from the encoder, so our approach is not affected by the nonlinearity of the machine and inverter. Firstly, the relation between torque ripple and speed harmonic is investigated and modeled. It is found that the magnitude of the speed harmonic is proportional to the magnitude of the torque harmonic of the same order. So,

Manuscript received April 15, 2016; revised August 22, 2016 and September 19, 2016; accepted October 8, 2016.

G. Feng, C. Lai and N. Kar are with the Department of Electrical and Computer Engineering, University of Windsor, Ontario, Canada. (email: guodong.feng, lai112, nkar@uwindsor.ca).

G. Feng is the corresponding author (phone: +1 519 253 3000 ext.5860; fax: +1 519 971 3695; e-mail: guodong.feng@uwindsor.ca).

the speed harmonic magnitude can be used as the feedback control signal to minimize the torque harmonic of the same order. To best of the authors' knowledge, it is the first time to investigate the use of the speed harmonic as a measure of the torque harmonic for torque ripple minimization. Then, the torque harmonic model considering the cogging torque and the magnet flux harmonic and current harmonic is proposed to investigate how the harmonic current influences the torque ripple to facilitate the design and analysis of the current controller. It shows that the torque harmonic is independent from machine speed, so the harmonic current designed for low speed is applicable to high speed. Finally, a novel fuzzy logic based controller is proposed to minimize the most dominant torque harmonic by using the magnitude of the speed harmonic of the same order as the feedback control signal. This is because the torque ripple is dominated by a small number of harmonics, so each harmonic can be minimized independently.

II. Torque Ripple Measure Using the Speed Harmonic Of The Same Order

The mechanical equation of PMSMs is expressed as

$$T_e - T_L = J\frac{d\omega_m}{dt} + B\omega_m \tag{1}$$

where T_e is output torque of a PMSM, T_L is the load torque, J is the combined moment of inertia, B is the viscous friction coefficient, ω_m is the rotor mechanical speed.

From (1), the torque harmonic produced by a PMSM will induce the speed harmonic of the same order. To this end, the torque and speed are decoupled in the dc and harmonic terms as in (2) and (3).

$$T_e = T_{e0} + \sum_k T_{ek}\cos(k\theta - \phi_{ek}) \tag{2}$$

$$\omega_m = \omega_{m0} + \sum_k \omega_{mk}\cos(k\theta - \phi_{\omega k}) \tag{3}$$

where T_{e0} is the average torque, T_{ek} and ϕ_{ek} are the magnitude and phase angle of the k^{th} torque harmonic; ω_{m0} is the average speed, ω_{mk} and $\phi_{\omega k}$ are the magnitude and phase of the k^{th} speed harmonic; θ is rotor electrical position; k is the harmonic order.

Substituting (2) and (3) into (1) and assuming there is no harmonic in load torque, the results (4) and (5) are obtained.

$$T_{e0} - T_L = B\omega_{m0} \tag{4}$$

$$\begin{aligned} T_{ek}\cos(k\theta - \phi_{ek}) = {} & B\omega_{mk}\cos(k\theta - \phi_{\omega k}) \\ & - kJP\omega_{m0}\omega_{mk}\sin(k\theta - \phi_{\omega k}) \end{aligned} \tag{5}$$

where P is the number of pole pairs. Based on (5), the relation between the magnitude of the torque and speed harmonic is

$$T_{ek} = \omega_{mk}\sqrt{B^2 + \left(kJP\omega_{m0}\right)^2} \tag{6}$$

Here, B is far smaller than $kJP\omega_{m0}$, so (6) can be simplified as

$$T_{ek} = kJP\omega_{m0}\omega_{mk} \tag{7}$$

It can be seen from (7) that the k^{th} speed harmonic magnitude, ω_{mk}, is proportional to the k^{th} torque harmonic magnitude T_{ek} and inversely proportional to the machine speed ω_{m0}. Here, ω_{mk} can be obtained from the speed measurement, so it can be used as a measure of T_{ek} for torque ripple minimization, which is not influenced by the nonlinearity of machine and the drive.

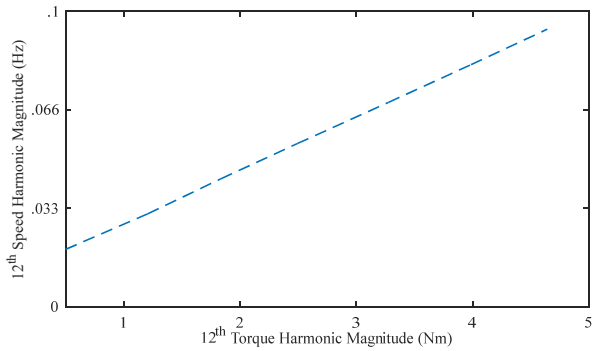

Fig.1. The relationship between torque harmonic magnitude T_{e12} and the speed harmonic magnitude ω_{m12}.

According to [16], the torque harmonics produced by a PMSM is dominated by a small number of harmonics such as the 6th and 12th harmonics. For the test PMSM, the 12th harmonic is the dominant torque harmonic. So the relationship between the 12th torque harmonic magnitude T_{e12} and 12th speed harmonic magnitude ω_{m12} is investigated and presented in Fig. 1, which agrees with the result of (7). In what follows, the ω_{m12} will be used as the feedback signal for current control to minimize the torque harmonic.

III. Torque Ripple Modeling And Minimization

The torque produced by a PMSM can be represented as [1]

$$T_e = \frac{3}{2}P\left((L_{dq}i_{dq} + \lambda_{dq})^T \times i_{dq} + i_{dq}^T\frac{d\lambda_{dq}}{d\theta}\right) + T_{cog} \tag{8}$$

where L_{dq}=diag$\{L_d, L_q\}$ is the dq-axis inductance matrix, $\lambda_{dq}=[\lambda_d\ \lambda_q]^{\mathrm{T}}$ and $i_{dq}=[i_d\ i_q]^{\mathrm{T}}$ are the dq-axis magnet flux vector and current vector, θ is the rotor electrical position, T_{cog} is the cogging torque, '×' is cross product defined as

$$[a\ b]\times[c\ \ d]^T = ad - bc \tag{9}$$

From (8), the torque harmonics are mainly caused by magnet flux harmonics, current harmonics and cogging torque. After a machine is designed, the magnet flux harmonic and cogging torque are uncontrollable. However, the stator current can be controlled to minimize torque ripples. More specifically, by injecting the properly designed current harmonics into the machine, the torque harmonic generated by the current harmonics can cancel the torque harmonics generated by the magnet flux harmonic and cogging torque. Therefore, we firstly model the torque harmonics induced by the magnet flux harmonic and cogging torque, and then discuss torque ripple minimization by injecting current harmonics.

The dq-axis magnet flux including harmonic components is expressed as (10) and the cogging torque is denoted as (11) [16, 30], where λ_0 is the dc component, λ_{dk} and λ_{qk} are the k^{th} magnet flux harmonic components and $\phi_{\lambda k}$ is the corresponding phase angle; T_{ck} is the k^{th} harmonic component in cogging torque and ϕ_{ck} is the corresponding phase angle.

$$\lambda_{dq} = \lambda_{dq0} + \sum_k \lambda_{dqk} = \begin{bmatrix}\lambda_0\\ 0\end{bmatrix} + \begin{bmatrix}\sum_k \lambda_{dk}\cos(k\theta - \phi_{\lambda k})\\ \sum_k \lambda_{qk}\sin(k\theta - \phi_{\lambda k})\end{bmatrix} \tag{10}$$

$$T_{cog} = \sum_k T_{ck}\cos(k\theta - \phi_{ck}) \tag{11}$$

This article has been accepted for publication in a future issue of this journal, but has not been fully edited. Content may change prior to final publication. Citation information: DOI 10.1109/TIE.2016.2631524, IEEE Transactions on Industrial Electronics

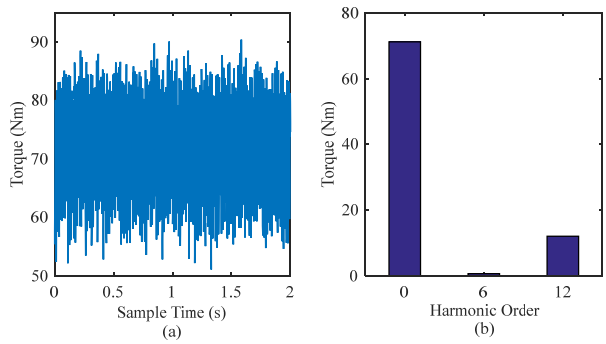

Fig. 2. The shaft torque of the test PMSM at rated torque condition. (a) Torque waveform. (b) Harmonic components.

Figure 2 shows the output torque of the test machine at rated torque condition. The torque ripple is dominated by the 12th harmonic, which occupies a major part of the total harmonics. Thus, we specifically consider to model and minimize the most dominant torque harmonic. Specifically, the 12th torque harmonic is used as the dominant torque harmonic in this paper. Therefore, in (10) and (11), the subscript "*k*" will take the value of 12. However, it should be noted that if the machine has two or more dominant torque harmonics, each one can be modeled independently by using the above model.

With this in mind, substituting (10) and (11) into (8) yields the total torque (12) including the average torque (13) and the 12th harmonic torque (14), where β and φ are given in (15) and (16), where i_{d0} and i_{q0} are the *dq*-axis dc currents.

$$T_e = T_{e0} + T_{e12m} \tag{12}$$

$$T_{e0} = \frac{3}{2} P\left(\lambda_0 i_{q0} + \left(L_d - L_q\right) i_{d0} i_{q0}\right) \tag{13}$$

$$T_{e12m} = \beta \cos(12\theta - \varphi) + T_{c12} \cos(12\theta - \phi_{c12}) \tag{14}$$

where

$$\beta = 1.5P\sqrt{i_{q0}^2\left(\lambda_{d12} + 12\lambda_{q12}\right)^2 + i_{d0}^2\left(\lambda_{q12} + 12\lambda_{d12}\right)^2} \tag{15}$$

$$\varphi = \phi_{\lambda 12} + \tan^{-1}\frac{-i_{d0}\left(\lambda_{q12} + k\lambda_{d12}\right)}{i_{q0}\left(\lambda_{d12} + k\lambda_{q12}\right)} \tag{16}$$

Here, the 12th torque harmonic T_{e12m} is caused by the magnet flux harmonic and cogging torque, so it is uncontrollable after the machine is designed.

However, the current harmonics can generate torque harmonics to cancel T_{e12m}. So, the stator currents are decoupled into two parts: one is the dc component that is used to produce the required torque, and the other is harmonic current that is used for torque ripple minimization. The *dq*-axis currents are decoupled as

$$i_{dq} = i_{dq0} + \sum_k i_{dqk} = \begin{bmatrix} i_{d0} \\ i_{q0} \end{bmatrix} + \begin{bmatrix} \sum_k i_{dk} \cos(k\theta - \phi_{ik}) \\ \sum_k i_{qk} \sin(k\theta - \phi_{ik}) \end{bmatrix} \tag{17}$$

where $i_{dq0}=[i_{d0}\ i_{q0}]^{\mathrm{T}}$ is the *dq*-axis dc currents, i_{dqk} is the k^{th} harmonic current, i_{dk} and i_{qk} are the harmonic current magnitudes and ϕ_{ik} is the phase angle.

As aforementioned, the 12th harmonic is dominant in torque ripple of the test machine, so the 12th harmonic current is considered, and (17) is simplified as (18).

$$i_{dq} = i_{dq0} + i_{dq12} = \begin{bmatrix} i_{d0} \\ i_{q0} \end{bmatrix} + \begin{bmatrix} i_{d12} \cos(12\theta - \phi_{i12}) \\ i_{q12} \sin(12\theta - \phi_{i12}) \end{bmatrix} \tag{18}$$

Substituting (18) into (8), the 12th torque harmonic produced by the current harmonic is given in (19), where the parameters α and ϕ are given in (20) and (21).

$$T_{e12c} = \alpha \cos(12\theta - \phi) \tag{19}$$

$$\alpha = 1.5P\sqrt{\left(\left(L_d - L_q\right) i_{q0}\right)^2 i_{d12}^2 + \left(\lambda_0 + \left(L_d - L_q\right) i_{d0}\right)^2 i_{q12}^2} \tag{20}$$

$$\phi = \phi_{i12} + \tan^{-1}\frac{\left(\lambda_0 + \left(L_d - L_q\right) i_{d0}\right) i_{q12}}{\left(L_d - L_q\right) i_{q0} i_{d12}} \tag{21}$$

Based on (14) and (19), the total 12th torque harmonic is

$$\begin{aligned} T_{e12} &= T_{e12m} + T_{e12c} \\ &= \alpha \cos(12\theta - \phi) + \beta \cos(12\theta - \varphi) + T_{c12} \cos(12\theta - \phi_{c12}) \end{aligned} \tag{22}$$

The objective of torque ripple minimization is to control the harmonic currents i_{dq12} so that T_{e12c} can cancel T_{e12m}, that is, to minimize the magnitude of T_{e12}. The harmonic current will generate the iron loss and copper loss which are approximately proportional to the square of the current magnitudes [16]. Therefore, it is desirable to reduce the magnitude of the designed harmonic current.

Ideally, we aim to minimize the torque harmonic magnitude to zero, that is, T_{e12}=0. According to (22), we have

$$\alpha \cos(12\theta - \phi) + \beta \cos(12\theta - \varphi) + T_{c12} \cos(12\theta - \phi_{c12}) = 0 \tag{23}$$

From (23), the result of (24) is obtained.

$$\alpha \cos(12\theta - \phi) = -\beta \cos(12\theta - \varphi) - T_{c12} \cos(12\theta - \phi_{c12}) \tag{24}$$

Considering only the magnitudes in (24), the result is

$$\begin{aligned} \alpha &= \sqrt{\left(\beta \cos\varphi + T_{c12} \cos\phi_{c12}\right)^2 + \left(\beta \sin\varphi + T_{c12} \sin\phi_{c12}\right)^2} \\ &= \sqrt{\beta^2 + T_{c12}^2 + 2\beta T_{c12} \cos(\varphi - \phi_{c12})} \end{aligned} \tag{25}$$

Based on (25), the harmonic current magnitude must satisfy

$$\alpha \le \sqrt{\beta^2 + T_{c12}^2 + 2\beta T_{c12}} = \beta + T_{c12} \tag{26}$$

Moreover, it can be seen from (20) that 1) the *d*-axis current harmonic will not generate torque ripple for surface-mounted PMSM, 2) for the same magnitude, the *d*-axis harmonic current will generate fewer torque ripple than the *q*-axis current for interior PMSM. Therefore, we consider injecting only the *q*-axis harmonic current, so (20) and (21) are simplified as

$$\alpha = \frac{3}{2} P\left(\lambda_0 + \left(L_d - L_q\right) i_{d0}\right) i_{q12} \tag{27}$$

$$\phi = \phi_{i12} + \frac{\pi}{2} \tag{28}$$

Substituting (27) into (26), i_{q12} must satisfy (29) and its phase angle should be within (30).

$$i_{q12} \le \frac{2\left(\beta + T_{c12}\right)}{3P\lambda_0 + 3P i_{d0}\left(L_d - L_q\right)} \tag{29}$$

$$\phi_{i12} \in [0, 2\pi] \tag{30}$$

From (22), both i_{q12} and ϕ_{i12} influence the magnitude of the 12th torque harmonic. So, the simulation is performed to investigate this influence. The result is given in Fig. 3, where i_{q12} varies from 1 to 3 A and ϕ_{i12} varies from π/2 to 3π/2. From Fig. 3, for a fixed i_{q12}, with the increase of ϕ_{i12}, the magnitude of T_{e12} decreases at first and then increases. When ϕ_{i12} is within [0.7π, 1.3π], for a fixed ϕ_{i12}, with the increase of i_{q12}, the magnitude of T_{e12} decreases at first and then increases. In what follows, a closed-loop fuzzy logic controller will be proposed for harmonic current control.

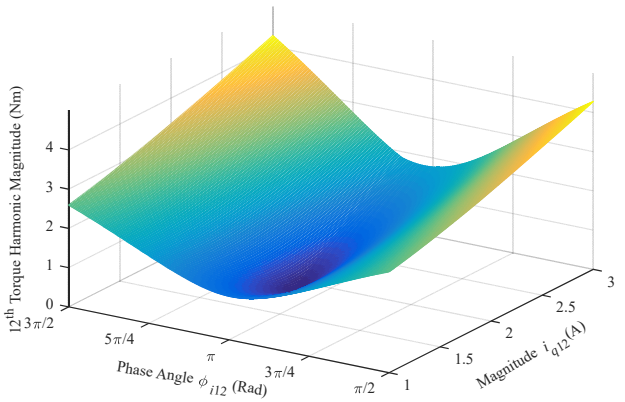

Fig.3. The relationship between the magnitude and phase angle of the *q*-axis 12th current harmonic and the magnitude of 12th torque harmonic.

IV. Closed-Loop Fuzzy-Logic Based Current Control

The main goal of the proposed fuzzy logic controller (FLC) is to control the harmonic current to minimize the magnitude of T_{e12} by using 12th speed harmonic magnitude as the feedback control signal. This is because the 12th speed harmonic magnitude is proportional to the magnitude of T_{e12}. Another objective is to minimize the magnitude of harmonic current to reduce the losses induced by the harmonic current.

The diagram of the proposed FLC is shown in Fig. 4. The input parameters of the proposed FLC are the magnitude of speed harmonic, ω_{m12}, and its derivative $\Delta\omega_{m12}$, as shown in (31) and (32), where t is the time instance and Δt is the sampling time. In actual implementation, instead of using FFT, a speed harmonic detection is employed to detect the speed harmonic, which will be detailed in experimental section.

$$\omega_{m12}(t) = \text{Harmonic\_Detection}\left(\omega_m(t)\right) \tag{31}$$

$$\Delta\omega_{m12}(t) = \frac{\omega_{m12}(t) - \omega_{m12}(t-1)}{\Delta t} \tag{32}$$

The outputs of the FLC are the magnitude and phase angle of the harmonic current, i_{q12} and ϕ_{i12}, which is used to minimize the magnitude of T_{e12}. Here, the outputs must satisfy the conditions of (29) and (30).

The FLC can be viewed as a mapping from the input linguistic variables (ω_{m12} and $\Delta\omega_{m12}$) to the output linguistic variables (i_{q12} and ϕ_{i12}), denoted as

$$u(t+1) = \text{FLC}\left(\omega_{m12}(t), \Delta\omega_{m12}(t)\right) \tag{33}$$

Here u includes the two output parameters i_{q12} and ϕ_{i12}.

In this paper, the proposed FLC employs a hierarchal control structure, in which the control of the current phase angle and magnitude is decoupled and they are controlled alternately until the torque harmonic magnitude is minimized. Specifically, at first, the proposed controller initializes a small current magnitude and regulates the phase angle until the speed harmonic magnitude is minimized. If the speed harmonic magnitude is within the acceptable lower level, the proposed controller will keep the phase angle and current magnitude. Otherwise, it will increase the current magnitude and then regulate the phase angle again to minimize the speed harmonic magnitude. The proposed controller will repeat the above control procedure until the speed harmonic is reduced to the acceptable lower level. Therefore, the torque harmonic is minimized as well, because its magnitude is proportional to the speed harmonic magnitude.

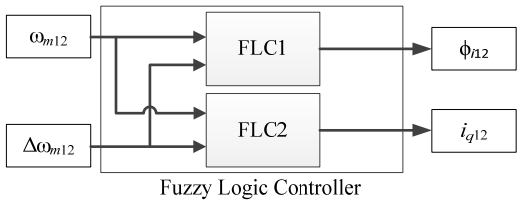

Fig.4. The diagram of the proposed hierarchal fuzzy logic controller (FLC).

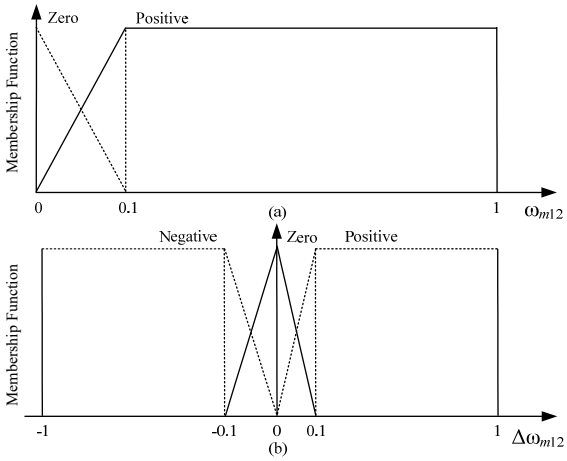

Fig.5. The membership functions. (a) Membership function of ω_{m12}. (b) Membership function of $\Delta\omega_{m12}$.

More specifically, as show in Fig. 4, the FLC consists of two separate controllers, namely, FLC1 and FLC2, as given in (34).

$$\begin{aligned} \phi_{i12}(t+1) &= \text{FLC1}\left(\omega_{m12}(t), \Delta\omega_{m12}(t)\right) \\ i_{q12}(t+1) &= \text{FLC2}\left(\omega_{m12}(t), \Delta\omega_{m12}(t)\right) \end{aligned} \tag{34}$$

The first controller, FLC1, focuses on controlling the phase angle ϕ_{i12}, and the second controller, FLC2, focuses on controlling the magnitude i_{q12}. In such a way, i_{q12} will be controlled to increase gradually until it reaches the minimal value required to minimize the magnitude of T_{e12}.

Each fuzzy logic controller consists of three modules, namely, *fuzzification*, *fuzzy inference*, and *defuzzification* modules. The task of *fuzzification* module is to covert the input variables, ω_{m12} and $\Delta\omega_{m12}$, into the corresponding linguistic variables. The task of *fuzzy inference* module is to obtain the control rules per the input linguistic variables. The task of *defuzzification* module is to translate the control rules into the reference values of the output variables i_{q12} and ϕ_{i12}.

The membership functions of the normalized variables ω_{m12} and $\Delta\omega_{m12}$ are shown in Fig. 5 (a) and (b), respectively. The variable ω_{m12} is decomposed into two fuzzy partitions, namely, *zero* and *positive*. The variable $\Delta\omega_{m12}$ is segmented into three partitions, namely, *negative*, *zero* and *positive*. The threshold value for each fuzzy partition is presented in Fig. 5. Here, there are some advantages of partitioning the input parameters with fewer linguistic terms. For instance, it can help to reduce the influence of the measurement noise on the controller.

In this paper, the Takagi-Sugeno type fuzzy inference system is adopted for current control. Specifically, the objective of the first controller FLC1 is to decrease the value ω_{m12} at time t by appropriately regulating the phase angle ϕ_{i12}. Therefore, the fuzzy control rules for FLC1 are as follows.

1. If ω_{m12} is *zero*, then keep ϕ_{i12}
2. If $\Delta\omega_{m12}$ is *zero*, then keep ϕ_{i12}

3. If ω_{m12} is *positive* and $\Delta\omega_{m12}$ is *positive*, then increase ϕ_{i12}
4. If ω_{m12} is *positive* and $\Delta\omega_{m12}$ is *negative*, then decrease ϕ_{i12}

The objective of the second controller FLC2 is to decrease the value ω_{m12} at time t by appropriately regulating the i_{q12}. Therefore, the fuzzy control rules for FLC2 are as follows.

5. If ω_{m12} is *zero*, then keep i_{q12}
6. If ω_{m12} is *positive* and $\Delta\omega_{m12}$ is *zero*, then increase i_{q12}
7. If ω_{m12} is *positive* and $\Delta\omega_{m12}$ is not *zero*, then keep i_{q12}

It should be noted that at the initial stage, the i_{q12} will be initialized with a small positive value such as five percent of the maximum magnitude as shown in (29).

It can be seen from rules 5-7 that the i_{q12} is updated by the FLC2 at time t only if when the optimal $\phi_{i12}(t\text{-}1)$ is obtained from FLC1 at time t-1. Therefore, the idea of the hierarchal FLC is that we firstly initialize i_{q12} and then find the optimal ϕ_{i12}. If the ω_{m12} is minimized then stop, otherwise increase i_{q12} and find the optimal ϕ_{i12} again. The i_{q12} and ϕ_{i12} will be iteratively updated until the optimal i_{q12} and ϕ_{i12} are found. It should be noted that the increase step of i_{q12} should be small so that the i_{q12} can gradually increase until it reaches the minimal value required for torque ripple minimization.

The magnitude of the harmonic current obtained from the controller FLC2 is the minimal magnitude required to minimize the torque ripple. We can prove it as follows. Suppose that there is a smaller magnitude i_{q12}^* that can minimize the torque ripple and the phase angle is ϕ_{i12}^*. The magnitude regulated by FLC2 increases gradually, so when i_{q12} increases to i_{q12}^*, FLC1 will output the optimal phase angle ϕ_{i12}^*. Therefore, when i_{q12}^* and ϕ_{i12}^* are obtained, the controller will converge to these two values.

The task of *defuzzification* is to determine the reference value of the magnitude and phase angle, i_{q12} and ϕ_{i12}, of the harmonic current from the control rules. To this end, we first compute the magnitude and phase angle by

$$\begin{aligned} \phi_{i12}(t+1) &= \phi_{i12}(t) + K_\phi(\omega_{m12}(t)) \\ i_{q12}(t+1) &= i_{q12}(t) + K_i(\omega_{m12}(t)) \end{aligned} \tag{35}$$

where K_ϕ and K_i denote the control gains. Here, the control gains in (35) are determined by the defuzzification rules as

8. Increase ϕ_{i12}: set $K_\phi>0$
9. Keep ϕ_{i12}: set $K_\phi=0$
10. Decrease ϕ_{i12}: set $K_\phi<0$
11. Increase i_{i12}: set $K_i>0$
12. Keep i_{i12}: set $K_i=0$

Then, the center-of-mass based approach is employed as the defuzzification method to compute the final current magnitude and phase angle, i_{q12} and ϕ_{i12}. It should be noted that the absolute value of the control gains, K_ϕ and K_i, should be small to ensure that the controller can find their optimal values. However, there is no general method for the selection of the control gains. In this paper, they are experimentally selected. As will be demonstrated in the experiments, selecting a larger control gain can result in a fast convergence speed. However, if the control gain is too large, it may miss the optimal solution. Therefore, the preferred selection method is that we select a small control gain at first and then increase the control gain gradually until it achieves the desired dynamic responses.

It should be noted that the magnitude and phase angle should comply with their bounds as indicated in (29) and (30). Therefore, the following two rules should be applied to the current magnitude and phase angle after defuzzification.

13. If $\phi_{i12}>2\pi$, then $\phi_{i12}= \phi_{i12}-2\pi$
14. If $i_{q12}> i_{q12max}$, then $i_{q12}=i_{q12max}$

where i_{q12max} is the maximum magnitude obtained from (29).

It should be noted that the magnitude of the torque harmonic is depending on the stator current, so when the stator current changes, the harmonic current should be reinitialized. In summary, the proposed FLC is detailed in Algorithm 1 as follows:

Algorithm 1: Fuzzy Logic Controller

1. Initialize i_{q12} and ϕ_{i12}
2. Use membership functions to calculate ω_{m12} and $\Delta\omega_{m12}$
3. Find the fuzzy control rules for i_{q12} and ϕ_{i12} from the rules 1-7 using the fuzzy values of ω_{m12} and $\Delta\omega_{m12}$
4. Use defuzzification rules 8-12 to find the control gains
5. Use defuzzification strategy to compute the reference values of i_{q12} and ϕ_{i12}
6. Use rule 15 to update ϕ_{i12}
7. Use defuzzification rules 13-14 to bound i_{q12} and ϕ_{i12}
8. Update ω_{m12} and $\Delta\omega_{m12}$ and go to 2

Here, the rule 15 will be generalized in experimental section.

TABLE I: THE FEA PARAMETERS OF THE TEST INTERIOR PMSM

Rated current	15 A	Rated voltage	275 V	*d*-axis inductance	30.4 mH
Rated speed	575 rpm	Magnet flux	0.67 Wb	*q*-axis inductance	87.5 mH
Rated Torque	70 Nm	Number of pole pairs	4	Number of Slots	48

V. Experimental Investigations

The proposed FLC is tested on an interior PMSM drive system as shown in Fig. 6, where the test PMSM is controlled by a real-time controller and the dyno motor is independently controlled that can deliver the desired speed or torque. The detailed design parameters of the test motor are listed in Table I. The test motor is designed for direct-drive electric vehicle application. A torque sensor is installed to measure the torque up to 100 Nm with a resolution of 0.1%. The shaft torque at no-load condition is given in Fig. 7 and the shaft torque at rated torque condition has been given in Fig. 2, where the shaft torque is measured by the torque transducer. The speed harmonic is used for feedback current control for torque ripple minimization. Therefore, using high-resolution encoder can improve the performance of the proposed approach. In the test machine, the employed high resolution optical encoder has a cycle per revolution of 2500. The speed harmonic obtained from encoder is used to minimize the torque harmonic.

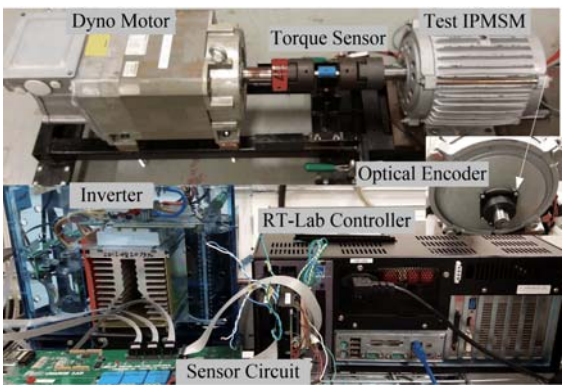

Fig. 6. Experimental setups for torque ripple minimization.

This article has been accepted for publication in a future issue of this journal, but has not been fully edited. Content may change prior to final publication. Citation information: DOI 10.1109/TIE.2016.2631524, IEEE Transactions on Industrial Electronics

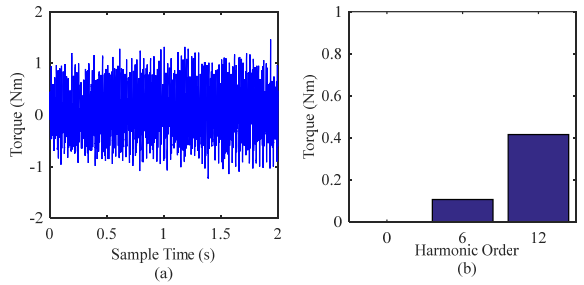

Fig.7. The shaft torque measured at no-load condition. (a) Torque waveform. (b) Harmonic components.

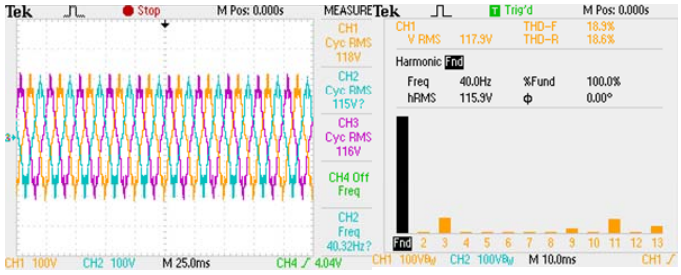

(a) (b)

Fig. 8. The back-EMF test results. (a) The three-phase open-circuit phase voltages. (b) The harmonic components of phase voltage in rms values.

At first, the back-EMF test is conducted to obtain the magnet flux components for calculation of the upper bound of the harmonic current with (29). The open-circuit phase voltage and its harmonic components are given in Fig. 8. The phase voltage has higher 3rd, 9th, 11th, 13th harmonics, so the magnet flux in *abc*-axis has the same order of harmonics. In order to obtain the *dq*-axis magnet flux, the magnet flux in the *abc*-axis is firstly estimated from the back-EMF test, and the park transformation is then applied to the magnet flux in the *abc*-axis. Specifically, the magnet flux in *abc*- axis is denoted as

$$\begin{cases} \lambda_a = \sum_k \lambda_{abc,k} \cos(k\theta) \\ \lambda_b = \sum_k \lambda_{abc,k} \cos\left(k\left(\theta - 2\pi/3\right)\right) \\ \lambda_c = \sum_k \lambda_{abc,k} \cos\left(k\left(\theta + 2\pi/3\right)\right) \end{cases} \quad (36)$$

where λ_a, λ_b and λ_c are the *abc*-axis magnet flux; $\lambda_{abc,k}$ is the magnitude of the k^{th} harmonic component, k is the harmonic order that can take values from {1,3,5,7…}.

Applying park transformation to (36), magnet flux in *dq*-axis is obtained as in (37), where $\lambda_0=\lambda_{abc,1}$ is the dc component, and k is the harmonic order taking values from {6, 12, …}.

$$\begin{cases} \lambda_d = \lambda_0 + \sum_k \left(\lambda_{abc,k-1} + \lambda_{abc,k+1}\right)\cos(k\theta) \\ \lambda_q = \sum_k \left(\lambda_{abc,k+1} - \lambda_{abc,k-1}\right)\sin(k\theta) \end{cases} \quad (37)$$

The control diagram is given in Fig. 9(a), in which the proposed FLC is integrated into the machine drive to control the 12th harmonic current. There are two independent current controllers: one is the PI controller that is used to control the *dq*-axis dc currents to follow the current reference for machine control, and the other is the proportional resonant (PR) controller that is used to control the harmonic current to follow the desired harmonic current reference obtained from the proposed FLC for torque ripple minimization. The outputs of the PI controller and PR controller are then added together to obtain the required *dq*-axis reference voltages.

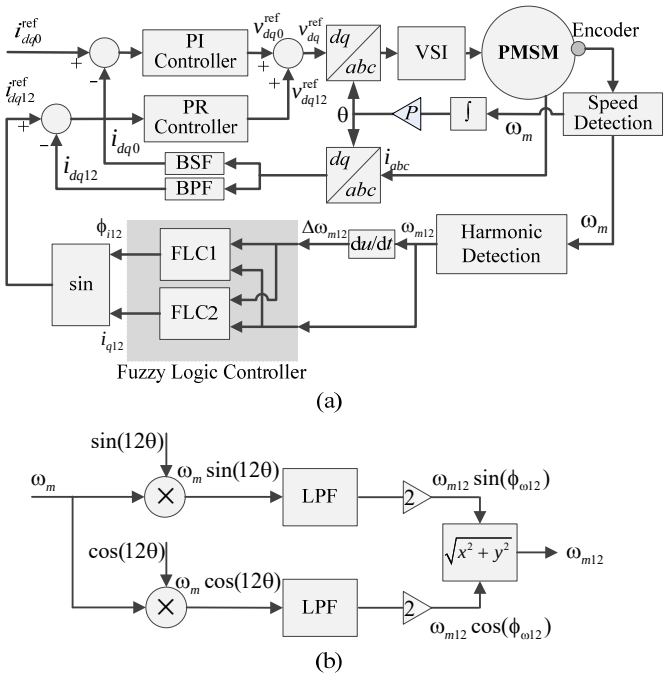

Fig. 9. The implementation diagram of the proposed fuzzy logic controller. (a) Machine control. (b) Speed harmonic detection. LPF: low-pass filter, BSF: band-stop filter, and BPF: band-pass filter.

TABLE II: EXPERIMENTAL SETUPS AND EXPLANATIONS

	Load (Nm)	Speed (rpm)	Gains		Objectives
			K_i	K_ϕ	
Ex1	35	100	1e-3	1e-3	Study how Rule 15 affects control performance
Ex2	35	100	Vary	Vary	Study how control gain affects convergence speed
Ex3	Vary	100	1e-2	1e-2	Study how load condition affects convergence speed
Ex4	35	Vary	1e-2	1e-2	Study how motor speed affects control performance

In the FLC, a computationally efficient speed harmonic detection block in Fig. 9(b) is employed to detect the 12th speed harmonic magnitude. At first, the speed measurements are multiplied by sin(12θ) and cos(12θ), and then the low-pass-filter (LPF) is applied to the results to obtain $0.5\omega_{m12}\sin(\phi_{\omega 12})$ as well as $0.5\omega_{m12}\cos(\phi_{\omega 12})$. Finally, with the mathematical operations in Fig. 9(b), the speed harmonic magnitude, ω_{m12}, can be obtained. The ω_{m12} and its derivative $\Delta\omega_{m12}$ are then fed to the FLC to produce the desired 12th harmonic current to minimize the 12th torque harmonic.

Four experiments (Ex1-Ex4) are conducted to evaluate the performance and feasibility of the proposed FLC under different load conditions and speeds. In the tests, the sampling time is $2e^{-5}$ second and the PWM frequency is 5 kHz. Details about each test are listed in Table II, in which the load torque, motor speed, control gains, and objectives are given.

A. *Experimental Results of Ex1*

In Ex1, the load torque is about 35 Nm with *dq*-axis reference currents being 0 and 10 A, respectively. The motor is running at 100 rpm. The control gains in (35) are set to be $K_\phi=K_i$=1e-3. The objective is to investigate how the rule 15 influences the control performance. Here the rule 15 will be summarized from this experiment.

Fig. 10(a) and (b) present the two input linguistic variables of the FLC, and Fig.10 (c) and (d) show the output control

This article has been accepted for publication in a future issue of this journal, but has not been fully edited. Content may change prior to final publication. Citation information: DOI 10.1109/TIE.2016.2631524, IEEE Transactions on Industrial Electronics

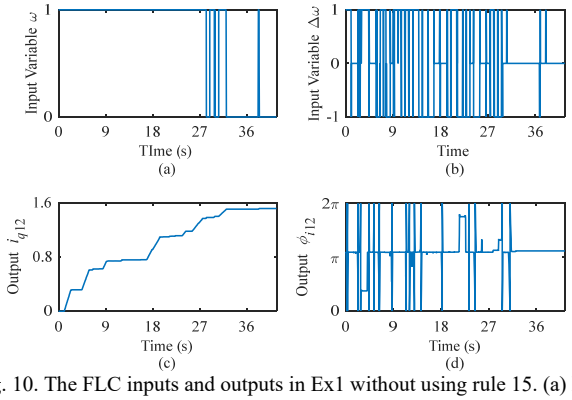

Fig. 10. The FLC inputs and outputs in Ex1 without using rule 15. (a) Input variable ω. (b) Input variable Δω. (c) Output i_{q12}. (d) Output ϕ_{i12}.

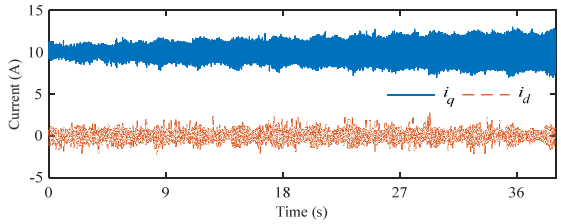

Fig. 11. The *dq*-axis currents in in Ex1 without using rule 15.

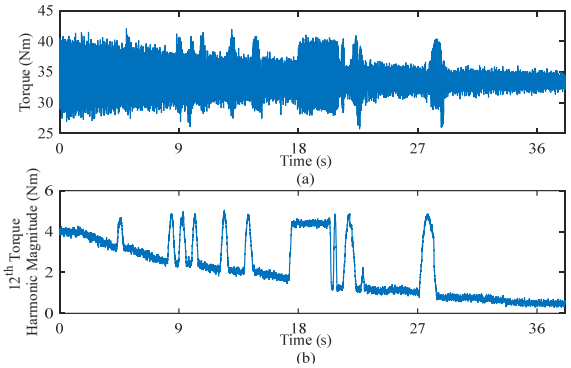

Fig. 12. The measured torque in Ex1 without using rule 15. (a) Torque waveform. (b) The 12th torque harmonic magnitude.

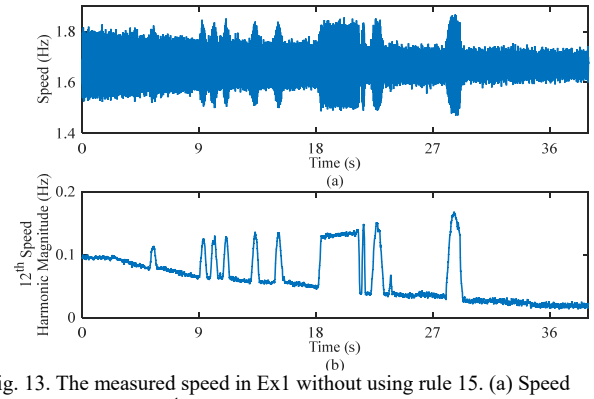

Fig. 13. The measured speed in Ex1 without using rule 15. (a) Speed waveform. (b) The 12th speed harmonic magnitude.

parameters including the magnitude and phase angle of the 12th harmonic current. From Fig. 10, after 36 seconds, the inputs of the FLC become zero, and the outputs converge to the optimal magnitude and phase angle, and they are 1.5 A and 196 degree. The *dq*-axis current is shown in Fig. 11, in which the magnitude of the *q*-axis harmonic current is increasing gradually. Here, the *q*-axis harmonic current is controlled by the FLC, in which its magnitude is controlled to increase gradually until the torque ripple is minimized. In other words, the increase of harmonic current is the result of the control action of the proposed controller. As can be seen from Fig. 11,

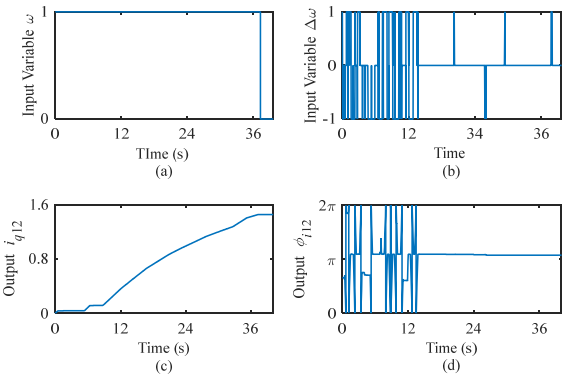

Fig. 14. The FLC inputs and outputs in Ex1 using rule 15. (a) Input variable ω. (b) Input variable Δω. (c) Output i_{q12}. (d) Output ϕ_{i12}.

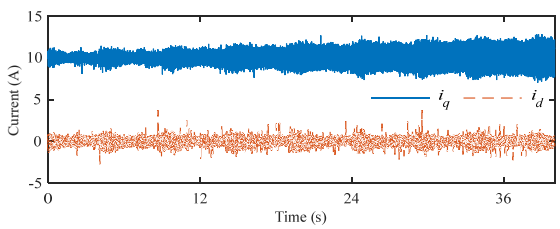

Fig. 15. The *dq*-axis currents in Ex1 using rule 15.

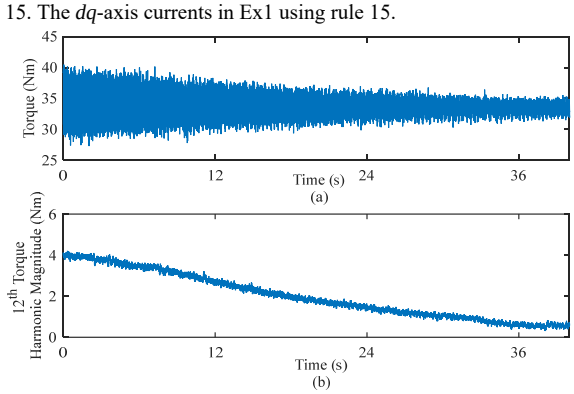

Fig.16. The measured torque in Ex1 using rule 15. (a) Torque waveform. (b) The 12th torque harmonic magnitude.

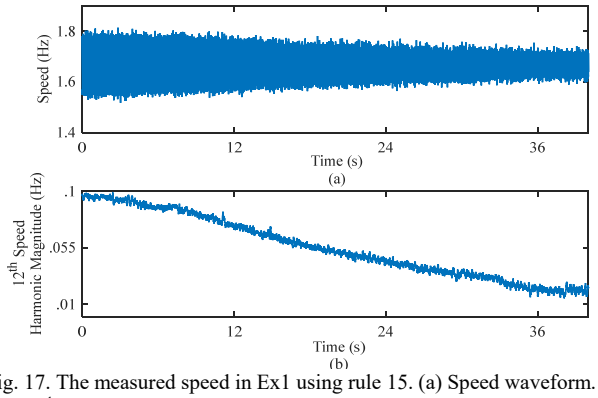

Fig. 17. The measured speed in Ex1 using rule 15. (a) Speed waveform. (b) The 12th speed harmonic magnitude.

after the torque ripple is minimized, the *q*-axis harmonic current will remain the same. However, the harmonic current does not influence the steady-state performance. Fig. 12 presents the torque measured by the torque transducer and the magnitude of the 12th torque harmonic during the torque ripple minimization using the FLC. Fig. 13 presents the corresponding speed measurements from the encoder and the magnitude of the 12th speed harmonic. From Figs.12 and 13, the 12th torque harmonic magnitude is reduced from 4 to 0.35 Nm, and the 12th speed harmonic magnitude is reduced from 0.1 to 0.02. However, the 12th torque and speed harmonic

This article has been accepted for publication in a future issue of this journal, but has not been fully edited. Content may change prior to final publication. Citation information: DOI 10.1109/TIE.2016.2631524, IEEE Transactions on Industrial Electronics

magnitudes are oscillating before convergence, which is not desired in applications. The reason is that when the harmonic current magnitude is increased, the controller will search the phase angle within 0-2π again until reaches the optimal one.

In order to eliminate this oscillating effect, we need to reset the searching space of the phase angle. It is found that at a specific operation condition, the optimal angle is independent from the magnitude of the harmonic current. Based on this, when the magnitude of the harmonic current is larger than a threshold, the phase angle is set to be the angle obtained at previous steps, which is summarized into the control rule 15 as:

15. If $i_{q12}>\varepsilon$, then set ϕ_{i12} to be the optimal value obtained at previous step and ignore other rules attempting to regulate ϕ_{i12}.

Here ε is a threshold, and it can be set to be the 40% of the maximum value of the harmonic current magnitude in (29).

After the rule 15 is included in the proposed FLC, the Ex1 is rerun and the results are as follows. Fig. 14 presents the inputs and outputs of the FLC. After i_{q12} is larger than 0.5 A, the phase angle is fixed to the value of 193 degree, which is followed by rule 15. Fig.15 shows the *dq*-axis current during the experiment. Figs. 16 and 17 present the torque and speed and their 12th harmonic magnitudes by using the rule 15. From these two figures, the oscillation in torque and speed harmonic is eliminated and the magnitude of the 12th torque and speed harmonic is gradually decreasing. Thus, the control performance has been improved by involving the rule 15.

B. Experimental Results of Ex2

In Ex2, the operation condition of the test PMSM is the same as that in the first experiment. However, the control gains in (32) are varying from (G1: K_ϕ=K_i=1e-2), (G2: K_ϕ=K_i=5e-3) to (G3: K_ϕ=K_i=1e-3), which aims to investigate how the control gains influence the convergence speed of the proposed FLC. Fig. 18 presents the 12th speed and torque harmonic magnitudes by using the FLC with different control gains. For G1, it takes five seconds for minimization; for G2, it takes ten seconds for minimization; and for G3, it takes 45 seconds for minimization. Therefore, the FLC convergence speed is increasing with the increase of control gain. However, a sudden increase of harmonic current may affect the drive dynamic performance, so a careful selection is necessary.

C. Experimental Results of Ex3

In Ex3, the test motor is operating at 100 rpm and the control gains are set to K_ϕ= K_i=1e-2, but the load torque is changed to 20 Nm and 70 Nm, which is to investigate how the proposed FLC performs at different load conditions.

Figs. 19 and 20 present the torque and speed and their 12th harmonic magnitudes when the load torque is about 70 Nm. It can be seen from these two figures that the 12th torque harmonic magnitude is reduced from 12 Nm to 0.4 Nm, and the 12th speed harmonic is reduced from 0.216 to 0.015. Moreover, it takes about 12 seconds for our FLC to minimize the torque harmonic. Fig. 21 (a) and (b) present the torque and the 12th torque harmonic magnitude when the load torque is 20 Nm. It takes about six seconds to reduce the 12th torque harmonic magnitude from 2.2 Nm to 0.4 Nm. With the increase of load torque, the convergence time of the proposed approach is slightly increased. One reason is that the torque harmonic magnitude is increasing with the increase of load torque. However, from Ex3, FLC is effective for torque ripple minimization under different load conditions.

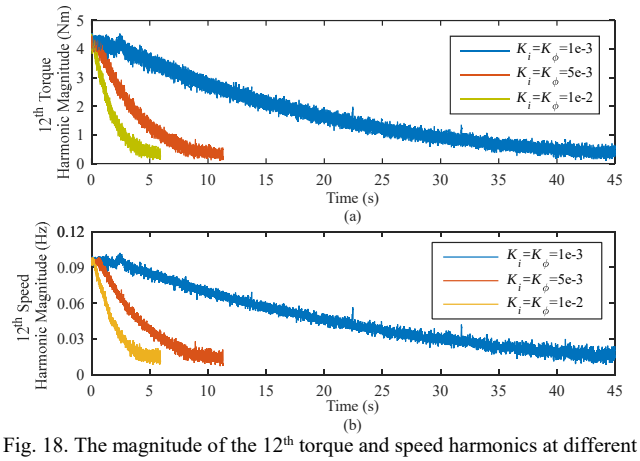

Fig. 18. The magnitude of the 12th torque and speed harmonics at different control gains in Ex2. (a) Torque Harmonic. (b) Speed Harmonic.

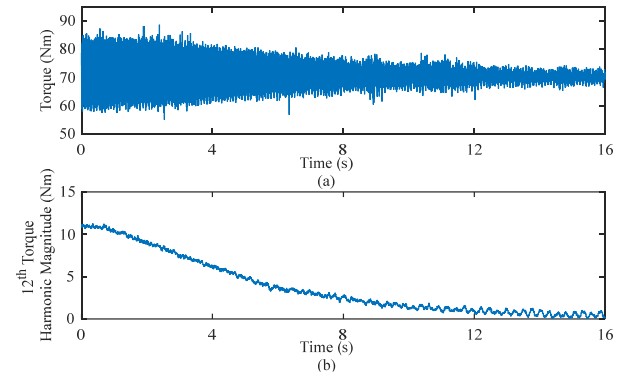

Fig. 19. The torque in Ex3 obtained from torque sensor with a load torque of 70 Nm. (a) Torque waveform. (b) The 12th torque harmonic magnitude.

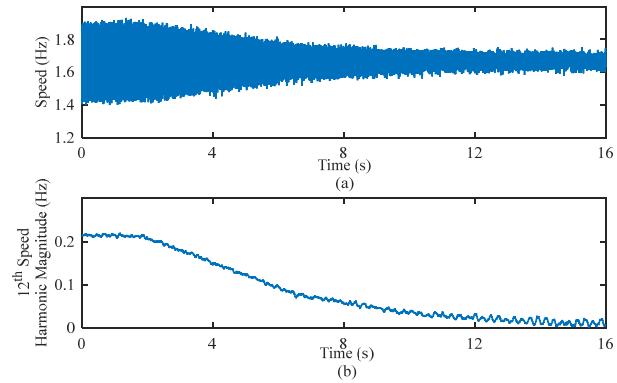

Fig. 20. The speed in Ex3 obtained from encoder. (a) Speed waveform. (b) The 12th speed harmonic magnitude.

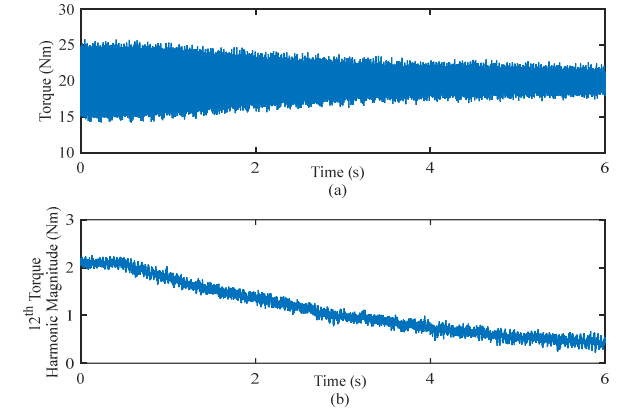

Fig. 21. The torque in Ex3 obtained from torque sensor with a load torque of 20 Nm. (a) Torque waveform. (b) The 12th torque harmonic magnitude.

This article has been accepted for publication in a future issue of this journal, but has not been fully edited. Content may change prior to final publication. Citation information: DOI 10.1109/TIE.2016.2631524, IEEE Transactions on Industrial Electronics

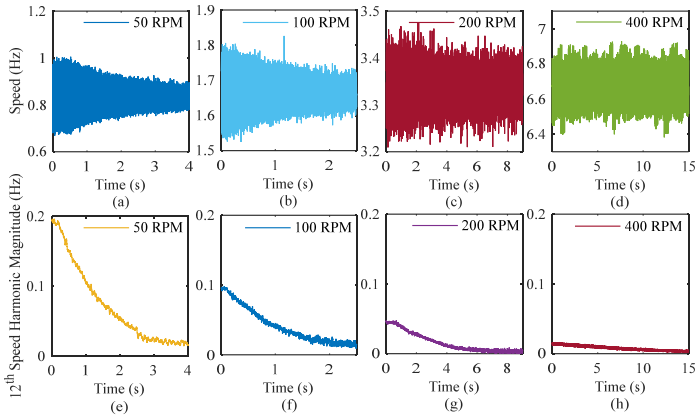

Fig. 22. The motor speed and its 12th harmonics magnitude at different motor speeds. (a) 50 rpm. (b) 100 rpm. (c) 200 rpm. (d) 400 rpm. (e) 12th speed harmonic at 50 rpm. (f) 12th speed harmonic at 100 rpm. (g) 12th speed harmonic at 200 rpm. (h) 12th speed harmonic at 400 rpm.

TABLE III: OPTIMAL HARMONIC CURRENT AT DIFFERENT SPEED

	Optimal Parameters	
	i_{q12} (A)	ϕ_{i12} (degree)
50 rpm	1.53	197
100 rpm	1.5	193
200 rpm	1.49	195
400 rpm	1.51	189

D. *Experimental Results of Ex4*

In Ex4, the load torque is 35 Nm, which is the same as that in Ex1 and Ex2 and the control gains are K_ϕ=K_i=1e-2. However, the operating speeds of the test PMSM is varying from 50 to 400 rpm, which is to study how the proposed FLC performs under different speeds. Fig. 22 presents the motor speed and its 12th harmonic magnitude at different speeds. From Fig. 22, at 50 rpm, the 12th speed harmonic magnitude is reduced from 0.2 to 0.018 in 4 seconds; at 100 rpm, it is reduced from 0.1 to 0.014 in 5 seconds; at 200 rpm, it is reduced from 0.0456 to 0.004 in 8 seconds; at rated speed, it is reduced from 0.0146 to 0.0044 in 28 seconds. With the same control gain, the convergence speed at high speed is decreasing due to the decrease of 12th speed harmonic magnitude. This is because with the increase of motor speed, the 12th speed harmonic magnitude is decreasing because it is inversely proportional to the motor speed. Thus, larger control gains are preferred at higher speed to increase the convergence speed. These results demonstrate that our FLC is effective from lower speed to high speed for the test PMSM.

The harmonic current parameters at each speed are given in Table III. It can be seen that the required harmonic current at each speed are similar. This is because torque harmonic model does not contain any term related to the machine speed. So, when the stator currents remain the same, the harmonic current obtained at lower speed are applicable to high speed.

VI. Discussions and Conclusions

The proposed approach requires the order of the dominant torque harmonic before applying to a new machine. A simple way is to apply a FFT to the speed measurements of the test machine to obtain this information. The speed measurements are generally available in a PMSM drive, so the proposed approach can be flexibly extended to other PMSMs. Indeed, the above harmonic order detection can be combined into the proposed approach as an initialization step.

The proposed approach uses the speed harmonic as the feedback control signal, so it is effective if the speed harmonic can be accurately detected. The harmonic detection block in Fig. 9(b) is still effective when the speed goes through a slow speed transient. However, if the speed changes too fast, the speed harmonic detection becomes challenging. Therefore, it is preferable to operate the proposed approach at steady state.

This paper proposed a novel closed-loop fuzzy logic based current controller for PMSM torque ripple minimization. The proposed controller does not involve much computation, which is critical for practical implementation. It does not require offline training and accurate information of the test machine, so extending it to other machines can be easily achieved. Moreover, a proper selection of the parameter partition can help to reduce the influence from the measurement noise. In this paper, the relation between torque ripple and speed harmonic of the same order is investigated and modeled to show that the speed harmonic magnitude can be applied for torque ripple minimization. The torque harmonic model is proposed to show that the torque harmonic is mainly depending on the stator fundamental currents and independent from machine speed. This result is significant because the speed harmonic magnitude is inversely proportional to the motor speed, so it is unable to ensure a high signal to noise ratio at high speed, but we can apply the harmonic current obtained at low speed to high speed.

References

[1] N. Nakao and K. Akatsu, “Suppressing pulsating torques: Torque ripple control for synchronous motors,” *IEEE Ind. Appl. Mag.*, vol. 20, no. 6, pp. 33–44, Nov 2014.

[2] F. Betin, G.-A. Capolino, D. Casadei, B. Kawkabani, R. Bojoi, L. Harnefors, E. Levi, L. Parsa, and B. Fahimi, “Trends in electrical machines control: Samples for classical, sensorless, and fault-tolerant techniques,” *IEEE Ind. Electron. Mag.*, vol. 8, no. 2, pp. 43–55, June 2014.

[3] G. Feng, C. Lai, and N. Kar, “Expectation maximization particle filter and kalman filter based permanent magnet temperature estimation for PMSM condition monitoring using high-frequency signal injection,” *IEEE Trans. Ind. Informat.*, 2016, doi: 10.1109/TII.2016.2591509, in press.

[4] A. Gebregergis, M. Chowdhury, M. Islam, and T. Sebastian, “Modeling of permanent-magnet synchronous machine including torque ripple effects,” *IEEE Trans. Ind. Appl.*, vol. 51, no. 1, pp. 232–239, Jan 2015.

[5] Y. Xu, N. Parspour, and U. Vollmer, “Torque ripple minimization using online estimation of the stator resistances with consideration of magnetic saturation,” *IEEE Trans. Ind. Electron.*, vol. 61, no. 9, pp. 5105–5114, Sept 2014.

[6] C. Xia, B. Ji and Y. Yan, "Smooth Speed Control for Low-Speed High-Torque Permanent-Magnet Synchronous Motor Using Proportional–Integral–Resonant Controller," *IEEE Trans. Ind. Electron*, vol. 62, no. 4, pp. 2123-2134, April 2015.

[7] X. Chen, J. Hu, K. Chen, and Z. Peng. "Modeling of electromagnetic torque considering saturation and magnetic field harmonics in permanent magnet synchronous motor for HEV," *Simulation Modelling Practice and Theory*, vol.66 pp.212-225 Aug. 2016.

[8] P.H. Truong, D. Flieller, N. K. Nguyen, J. Mercklé, and G.Sturtzer, “Torque ripple minimization in non-sinusoidal synchronous reluctance motors based on artificial neural networks,” *Electric Power Systems Research* 2016.

[9] R. Islam, I. Husain, A. Fardoun, and K. McLaughlin, “Permanent-magnet synchronous motor magnet designs with skewing for torque ripple and cogging torque reduction,” *IEEE Trans. Ind. Appl.*, vol. 45, no. 1, pp. 152–160, Jan 2009.

[10] D. Wang, X. Wang, M.-K. Kim, and S.-Y. Jung, “Integrated optimization of two design techniques for cogging torque reduction combined with analytical method by a simple gradient descent method,” *IEEE Trans. Magn.*, vol. 48, no. 8, pp. 2265–2276, Aug 2012.

[11] D. Flieller, N. K. Nguyen, P. Wira, G. Sturtzer, D. Abdeslam, and J. Merckle, "A self-learning solution for torque ripple reduction for nonsinusoidal permanent-magnet motor drives based on artificial neural networks," *IEEE Trans. Ind. Electron.*, vol. 61, no. 2, pp. 655–666, Feb 2014.

[12] M. Amirian, A. Rashidi, S. Saghaeian Nejad, and M. Mojiri, "Multiple reference frame control of permanent magnet synchronous motor with non-sinusoidal back emf using adaptive notch filter," *2015 23rd Iranian Conference on Electrical Engineering*, May 2015.

[13] X. Xiao and C. Chen, "Reduction of torque ripple due to demagnetization in pmsm using current compensation," *IEEE Trans. Appl. Supercond.*, vol. 20, no. 3, pp. 1068–1071, June 2010.

[14] T. Jahns and W. Soong, "Pulsating torque minimization techniques for permanent magnet ac motor drives-a review," *IEEE Trans. Ind. Electron.*, vol. 43, no. 2, pp. 321–330, Apr 1996.

[15] K. Jezernik, J. Korelic, and R. Horvat, "Pmsm sliding mode fpga-based control for torque ripple reduction," *IEEE Trans Power Electron.*, vol. 28, no. 7, pp. 3549–3556, July 2013.

[16] P. Chapman, S. Sudhoff, and C. Whitcomb, "Optimal current control strategies for surface-mounted permanent-magnet synchronous machine drives," *IEEE Trans. Energy Conver.*, vol. 14, no. 4, pp. 1043–1050, Dec 1999.

[17] P. Mattavelli, L. Tubiana, and M. Zigliotto, "Torque-ripple reduction in pm synchronous motor drives using repetitive current control," *IEEE Trans. Power Electron.*, vol. 20, no. 6, pp. 1423–1431, Nov 2005.

[18] W. Qian, S. Panda, and J.-X. Xu, "Torque ripple minimization in pm synchronous motors using iterative learning control," *IEEE Trans. Power Electron.*, vol. 19, no. 2, pp. 272–279, March 2004.

[19] K. Liu, Z. Zhu, and D. Stone, "Parameter estimation for condition monitoring of pmsm stator winding and rotor permanent magnets," *IEEE Trans. Ind. Electron.*, vol. 60, no. 12, pp. 5902–5913, Dec 2013.

[20] K. Liu and Z. Zhu, "Position-offset-based parameter estimation using the adaline nn for condition monitoring of permanent-magnet synchronous machines," *IEEE Trans. Ind. Electron.*, vol. 62, no. 4, pp. 2372–2383, April 2015.

[21] K. Liu and Z. Zhu, "Online estimation of the rotor flux linkage and voltage-source inverter nonlinearity in permanent magnet synchronous machine drives," *IEEE Trans. Power Electron.*, vol. 29, no. 1, pp. 418–427, Jan 2014.

[22] K. Liu, Z. Zhu, Q. Zhang, and J. Zhang, "Influence of nonideal voltage measurement on parameter estimation in permanent-magnet synchronous machines," *IEEE Trans. Ind. Electron.*, vol. 59, no. 6, pp. 2438–2447, June 2012.

[23] G. Bramerdorfer, S. Winkler, M. Kommenda, G. Weidenholzer, S. Silber, G. Kronberger, M. Affenzeller, and W. Amrhein, "Using fe calculations and data-based system identification techniques to model the nonlinear behavior of pmsms," *IEEE Trans. Ind. Electron.*, vol. 61, no. 11, pp. 6454–6462, Nov 2014.

[24] Y. Cho, K.-B. Lee, J.-H. Song, and Y. Lee, "Torque-ripple minimization and fast dynamic scheme for torque predictive control of permanent-magnet synchronous motors," *IEEE Trans. Power Electron.,* vol. 30, no. 4, pp. 2182–2190, April 2015.

[25] P. Beccue and S. Pekarek, "A coupled piezoelectric/single-hall-sensor position observer for permanent magnet synchronous machines," *IEEE Trans. Ind. Electron.*, vol. 54, no. 5, pp. 2389–2397, Oct 2007.

[26] P. Beccue, J. Neely, S. Pekarek, and D. Stutts, "Measurement and control of torque ripple-induced frame torsional vibration in a surface mount permanent magnet machine," *IEEE Trans. Power Electron.,* vol. 20, no. 1, pp. 182–191, Jan 2005.

[27] P. Beccue, J. Neely, S. Pekarek, and D. Stutts, "Utilization of a piezoelectric polymer to sense harmonics of electromagnetic torque," *IEEE Power Electron. Lett.,* vol. 1, no. 3, pp. 69–73, Sept 2003.

[28] S. Chai, L. Wang, and E. Rogers, "A cascade mpc control structure for a pmsm with speed ripple minimization," *IEEE Trans. Ind. Electron.*, vol. 60, no. 8, pp. 2978–2987, Aug 2013.

[29] W. Qian, S. Panda, and J. Xu, "Speed ripple minimization in pm synchronous motor using iterative learning control," *IEEE Trans. Energy Conver.*, vol. 20, no. 1, pp. 53–61, March 2005.

[30] L. Romeral, J. Urresty, J. Ruiz, A. Espinosa, "Modeling of surface-mounted permanent magnet synchronous motors with stator winding interturn faults," *IEEE Trans. Ind. Electron.*, vol.58, no.5, pp.1576-1585, May 2011

Guodong Feng (M'15) received the B.S. and Ph.D degrees from Sun Yat-sen University, Guangzhou, China, in 2010 and 2015, respectively. He is currently a Post-Doctoral Fellow in the Department of Electrical and Computer Engineering, University of Windsor, Ontario, Canada. His research interests include intelligent information processing and electrical machine design, control and testing.

Chunyan Lai (S'14) received the B.S. degree in engineering from Sun Yat-sen University, China, in 2010. Between 2010 and 2013, she spent two and a half years in the industry. She is currently working towards her PhD degree at the University of Windsor, Canada. Her research areas include modelling, control and testing of permanent magnet machines and switched reluctance machines.

Narayan C. Kar (SM'07) received the B.Sc. degree in Electrical Engineering from Bangladesh University of Engineering and Technology, Dhaka, Bangladesh, in 1992 and the M.Sc. and Ph.D. degrees in electrical engineering from Kitami Institute of Technology, Hokkaido, Japan, in 1997 and 2000, respectively. He is a professor in the Electrical and Computer Engineering Department at the University of Windsor, Canada where he holds the Canada Research Chair position in Electrified Transportation Systems. His research presently focuses on the analysis, design and control of electrical machines for electrified vehicle applications; testing and performance analysis of batteries and development of optimization techniques for hybrid energy management system.